PAPER

Check for updates

View Article Online
View Journal | View Issue

Silk fibroin-derived peptide directed silver nanoclusters for cell imaging†

Peng Gao, [ID] *[a] Hao Wang,[b] Guifu Zou [ID] [b] and Ke-Qin Zhang [ID] *[a]

Fluorescent silver nanoclusters (Ag NCs) that are capable of emitting green light have been synthesized using a peptide derived from the C terminal of silk fibroin heavy chain (CSH) *via* a one-pot, green, and facile synthesis method. The emission was also found to be stable at the excitation wavelength and the fluorescence quantum yield of Ag NCs was measured to be 1.1%. Matrix assisted laser desorption ionization time of flight mass spectrometry (MALDI-TOF MS) indicated the presence of a range of Ag species that correspond to Ag1, Ag2, Ag3 and Ag4. Transmission electron microscopic analyses suggested that the formed particles are uniform and well dispersive with an average diameter of 2.5 nm. The Ag NCs were successfully applied to cell imaging in murine preosteoblast MC3T3-E1 cells. Finally, Ag NCs observed by MTT exhibited distinct cytotoxicity at CSH–Ag NCs concentrations of 600 μM. Based on the concept of utilizing a functional peptide from nature, this study demonstrates a novel approach to fabricate aqueous metal nanoclusters for tracking applications in bioimaging.

Introduction

Noble metal nanoclusters (NCs) have gained considerable attention for various applications in biological imaging, chemical sensing, catalysis and therapy due to their unique physical, electrical and optical properties.[1–4] Generally, metal NCs, comprising several to roughly dozens of metal atoms, are an emerging class of fluorescent materials, which are attracting increasing interests from many scientists. They possess discrete energy level and sizes that approach the Fermi wavelength of electrons and exhibit significant photoluminescence, which is regulated by their sub-nanometer dimensions. Compared to commonly used organic dyes, quantum dots and fluorescent proteins, metal NCs possess several unique characteristics, including tunable photo-properties, ultra-fine sub-nanometer size particles, high selectivity and high biocompatibility, enabling them as a highly attractive alternative for conventional probes. However, to the best of our knowledge, there is limited literature on Ag NCs and their applications, relative to that of Au NCs.[5,6] This is because silver clusters are more reactive than other metal analogues and tend to grow and form larger nanoparticles. As far as we know, ease of preparation, high quantum yield and high stability under physiological conditions are still the main challenges in the synthesis of Ag NCs. To reduce their surface energy, various chelating ligands, such as proteins, DNA, polymers, dendrimers, thiolates and other small molecules have been successfully used as stabilizing ligands for the synthesis of Ag NCs.[7–10]

Proteins/peptides serve as flexible and effective biotemplates, which have been demonstrated to have great potential for the controlled synthesis of metal NCs with characteristic biofunctions. In the case of peptide templates, Dickson *et al.* designed three short peptides from nucleolin with minor sequence differences to capture the silver clusters. These silver clusters exhibit similar photophysics to those in the nucleolus, but with narrower emissions at 610 nm (P1–Ag), 615 nm (P2–Ag), and 630 nm (P3–Ag). MALDI mass spectrometry confirms the presence of silver clusters and their composition, in which Ag2, Ag3, Ag4, or Ag5 are bound to a single peptide.[11] In the case of BSA, the synthesis of fluorescent BSA-Ag15 has been accomplished by using denatured BSA as a stabilizing agent and $NaBH_4$ as a reduction agent. The stability of BSA-Ag15 could be further enhanced by the addition of poly(vinyl pyrrolidone) in aqueous solution.[12] Furthermore, Xie *et al.* prepared gold nanoclusters of five discrete sizes (Au4, Au8, Au10, Au13, and Au25) by using BSA with a predefined protein conformation.[13] In conclusion, it has been demonstrated that the protein sequence and conformation as well as the protein size and amino acid content play key roles in controlling the size of the NCs, thus resulting in the formation of metal NCs with different sizes and varied fluorescence properties. Notably, certain proteins/peptides with distinct biological functions and characteristic sequence and conformation were demonstrated and predicted.[14,15] Currently, numerous proteins/peptides, including GSH,[16,17] lysozyme,[18] α-chymotrypsin,[19]

[a]National Engineering Laboratory for Modern Silk, College of Textile and Clothing Engineering, Soochow University, Suzhou, 215123, P. R. China. E-mail: pgao116@126.com; kqzhang@suda.edu.cn

[b]College of Physics, Optoelectronics and Energy, Collaborative Innovation Center of Suzhou Nano Science and Technology, Soochow University, Suzhou 215006, P. R. China

† Electronic supplementary information (ESI) available. See DOI: 10.1039/c8ra04607g
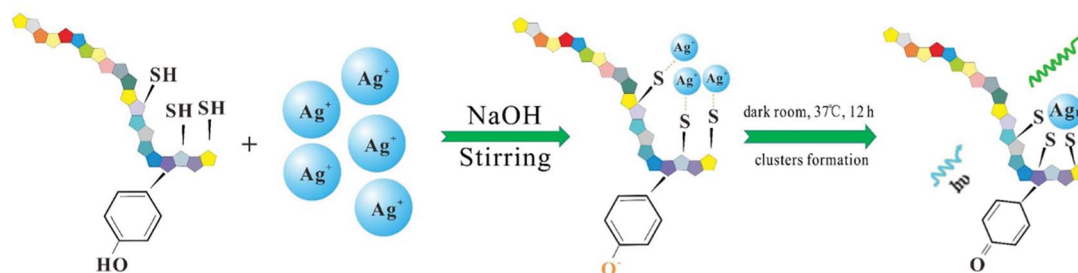
Scheme 1 Schematic of the synthesis of CSH–Ag NCs.

BSA,[20] HAS,[21] and programed peptides,[22,23] have been successfully adopted as novel biotemplates for the synthesis of Ag NCs. Nevertheless, only a few studies of Ag NCs have been reported using peptide/protein as the capping reagent.

To further explore the potential of silk fibroin and its derivatives, we initially employed one characteristic peptide of silk fibroin to fabricate hydrosoluble fluorescent Ag NCs. As shown in Scheme 1, CSH–Ag NCs with green emission were synthesized *via* a one pot, facile and green method. The characteristic peptide comprising 58 amino acids was selected from the C terminus of heavy chain of silk fibroin, featuring three cysteine units, four tyrosine units, and nine basic amino acids. Recent studies have shown that the presence of a thiol group (in cysteine) could facilitate the synthesis of peptide-protected metal NCs with good stability in solution due to the unique metal–sulfur chemistry that is typically strong.[22,24] We speculate that the peptide could be a potential biotemplate candidate for the synthesis of Ag NCs due to the presence of cysteine, tyrosine and basic amino acids. We observed that the CSH–Ag NCs with green emission can easily penetrate the cytomembrane, and hence can be effectively applied for cellular imaging.

Experimental

2.1. Materials

The chemically synthesized peptide was purchased from ChinaPeptides Co., Ltd., according to the pristine sequence data from NCBI, termed as CSH peptide (VSYGAGRGYGQGAGSAASSVSSASSRSYDYSRRNVRKNCGIPRRQLVVKFRALPCVNC, HPLC purified: 90%). Chlorauric acid was purchased from National Medicines Chemical Reagent Co., Ltd. (Shanghai, China). All reagents were of analytical grade and used without further purification. Water (18.25 MΩ cm) used in all experiments was deionized by the Milli-Q Academic purification set (Millipore, Bedford, MA, USA).

2.2. Synthesis of CSH–Ag NCs

All glassware was washed with aqua regia and rinsed with ultrapure water. Typically, the synthesis was started with an aqueous $AgNO_3$ solution (32.4 μL, 25 mM, 37 °C), which was slowly added to CSH peptide solution (205 μL, 2 mM, 37 °C). Then, NaOH solution (0.5 M, 5 μL) was added to achieve a final pH value of ~10. After vigorous stirring for 5 min, the reaction was incubated in a baking oven at 37 °C for 12 h.

2.3. Characterization of CSH–Ag NCs

Ultraviolet-visible (UV-vis) absorption spectra were recorded using a Shimadzu UV-2450 spectrophotometer. All the photoluminescence (PL) spectra were recorded on a Fluoromax-4 spectrofluorometer (HORIBA Jobin Yvon Inc.) equipped with a 150 W xenon lamp as the excitation source. The composition of CSH–Ag NCs was analyzed using MALDI-TOF mass spectrometry on a Bruker micro TOF-Q system. The pure peptide and as-synthesized CSH–Ag NCs were simultaneously characterized in a positive linear model using α-cyano-4-hydroxycinnamic acid (CHCA) as a matrix. Transmission electron microscopy (TEM) images were obtained on a FEI Tecnai F-20 microscope operating at 200 kV for measuring the nanostructure and size distribution. The size distribution of CSH–Ag NCs was analyzed from TEM images using image J software (ImageJ1.44p, National Institutes of Health, U.S.A.). X-ray photoelectron spectra (XPS) were acquired with a Japan Kratos Axis Ultra HAS spectrometer using a monochromatic Al Kα source.

2.4. Cell culture and imaging

The murine osteoblastic MC3T3-E1 cells (preosteoblast cells) were obtained from the Medical College of Soochow University and maintained in our lab. The cells were expanded in an alpha minimum essential medium (α-MEM, Thermo Fisher Scientific, U.S.A.) containing 10% fetal bovine serum (FBS, Life Technologies, U.S.A.) and 1% penicillin/streptomycin (Life Technologies, U.S.A.) in 5% CO_2 humidified incubator at 37 °C. The medium was replaced every 48 h. After culturing in the growth medium until 80–90% confluence, the cells were harvested for further use.

2.5. Cytotoxicity

To assess the cytotoxicity, cell viability assays were carried out with an MTT assay according to the standard manufacturer protocol. MC-3T3 E1 cells (1×10^4 cells per well) were seeded in a 96-well microplate and grown in α-MEM for 24 h in the presence of 5% CO_2 at 37 °C. Then, various concentrations of Ag NCs (0–600 μM) were added to the cells and kept for 24 h in similar conditions. For the reaction, 7.0 μL of MTT was added to each well of the microplate and kept for 2 h for the formation of formazan. The control experiment was carried out in a similar

way with various amounts of peptide. All of the experiments were carried out in triplicate. The percentage of cell viability of the control was taken as 100%.

Results and discussion

3.1. Synthesis of CSH–Ag NCs

Highly fluorescent Au NCs using aprotinin in aqueous solution were synthesized *via* a facile one pot method. For the synthesis, the peptide solution was mixed with a similar volume of $AgNO_3$ aqueous solution under thorough stirring. Some of the Ag ions interacted with the thiol groups of the CSH peptide to form an intermediate product. When pH was adjusted to the desired value by adding 1 M NaOH solution, the phenolic group of Y converted into a negative phenolic ion that reduced Ag ions to Ag atoms. The color of the mixed solution turned from pale to brown, indicating the formation of Ag NCs.[22] The as-prepared CSH–Ag NCs showed significant fluorescence under UV illumination. They were kept in a refrigerator for further use. Overall, this CSH peptide performs the role of a protecting ligand for Ag clusters synthesis.

3.2. Characterization of the CSH–Ag NCs

The optical properties of the peptide–Ag clusters were further characterized by ultraviolet-visible (UV-vis) absorption spectroscopy. There were no distinct absorption peaks between 200–350 nm belonging to the Au clusters. A peak at 520 nm in a gradient absorption from 350 to 800 nm was present in the absorption spectrum and was designated as the peptide–Ag clusters (the red dash line in the inset of Fig. 1). The fluorescence spectrum was also characterized using a Fluoromax-4 spectrofluorometer, which showed that the peptide–Ag NCs (Fig. 1) have maximum excitation and emission peaks at 525 nm and 550 nm, respectively. The absorption maxima matched the excitation wavelength in photoluminescence spectra. The as-

prepared CSH–Ag NCs solution is transparent under visible light and exhibits green emission under UV light at 365 nm. As shown by the inset of Fig. 1, the lyophilized CSH–Ag NCs powder maintains the corresponding fluorescence emission under visible and UV light. It is notable that both samples were stable in their aqueous solutions and as powder when stored at 4 °C in a dark room for more than one month (Fig. S1 in the ESI†). The excitation-independent PL spectrum showed that peptide–Ag NCs exhibited intrinsic fluorescence at 550 nm with different excitation wavelengths from 400 to 525 nm (Fig. S2 in the ESI†). The as-synthesized CSH–Ag clusters possess a fluorescence quantum yield of about 1.1%. The quantum yield (QY) of the CSH–Ag NCs was obtained using a 405 nm Xe laser and calibrated with Rhodamin 6G (Sigma 252433, dye content: 99%), according to the emission peak area and absorbance of the peptide–Au clusters and Rhodamin 6G. Matrix-assisted laser desorption/ionization time of flight mass spectrometry (MALDI-TOF MS) is a general way to identify the well-defined composition of peptide–Ag NCs, including accurate number of Ag clusters and peptide coating outside the Ag NCs.[25] Peptide–Ag clusters and the pure peptide were characterized in positive ion mode using α-cyano-4-hydroxycinnamic acid (CHCA) as a matrix. The spectrum of the peptide–Ag clusters was composed of a series of intense peaks between 5.8–6.8k m/z. The representative mass spectrum with labeled peaks is shown in the inset of Fig. 2. The spacing between adjacent intense peaks could be matched with the m/z of one intact peptide with one missing silver atom. The peak of m/z 108 corresponds to the loss of Ag in MALDI-TOF MS studies. All intense peaks correspond to a cluster and the m/z of the intense peaks match the formula of Ag1, Ag2, Ag3 and Ag4 (Fig. 2a). Furthermore, no apparent peaks were observed between 6800–19 000 m/z, suggesting that the Ag NCs in aqueous solution was not coated by multiple peptides. As reported previously, biomolecules with the sequence specificity and structure of DNA and the peptide play key roles in determining the composition of the Ag clusters and their optical properties.[13,23,26] Compared to the results of the Dickson study, our results showed that the sequence dependent peptide affects the accurate formation of Ag NCs. Based on these results, we speculate that different compositions of Ag NCs can be achieved by engineering the sequence of the protein/peptide, particularly with the use of cysteine and basic amino acids as stabilizing reagents.[16,27] Thus far, a limited amount of research has been conducted towards the precise production of Ag NCs by using engineered peptides. Due to the limitation of high cost associated with long peptides, the hypothesis should be further verified *via* experiment by using simplified peptides. To characterize the morphology of peptide–Ag NCs, TEM measurements were performed, which indicated that the as-prepared Ag NCs were uniform in size. Furthermore, the mean diameter of CSH–Ag NCs was determined to be around 2.162 ± 0.67 nm by measuring the diameters of 116 samples (Fig. 2b and c), which is consistent with previous reports of Ag clusters possessing a small average size.[28,29] Further probing by HRTEM showed the presence of crystalline particles with a lattice spacing of 0.24 nm, corresponding to the (111) plane of Ag(0). Due to the presence of basic groups, the uniform
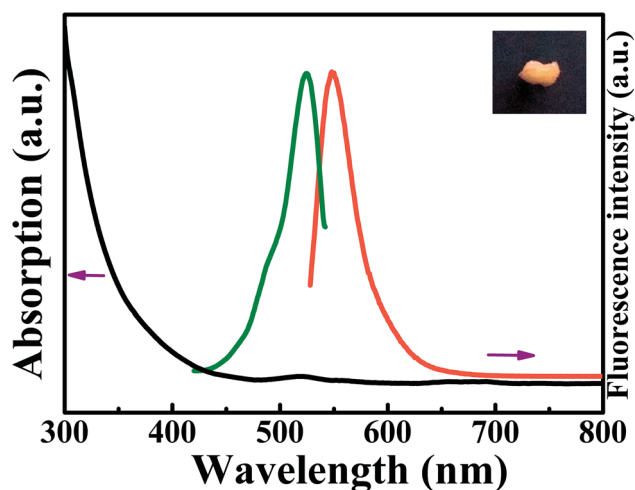

Fig. 1 UV-vis and fluorescence spectra of the as-prepared CSH–Ag NCs aqueous solution (black). Emission of CSH–Ag NCs at 550 nm excited at 525 nm spectra of the as-prepared CSH–Ag NCs aqueous solution.
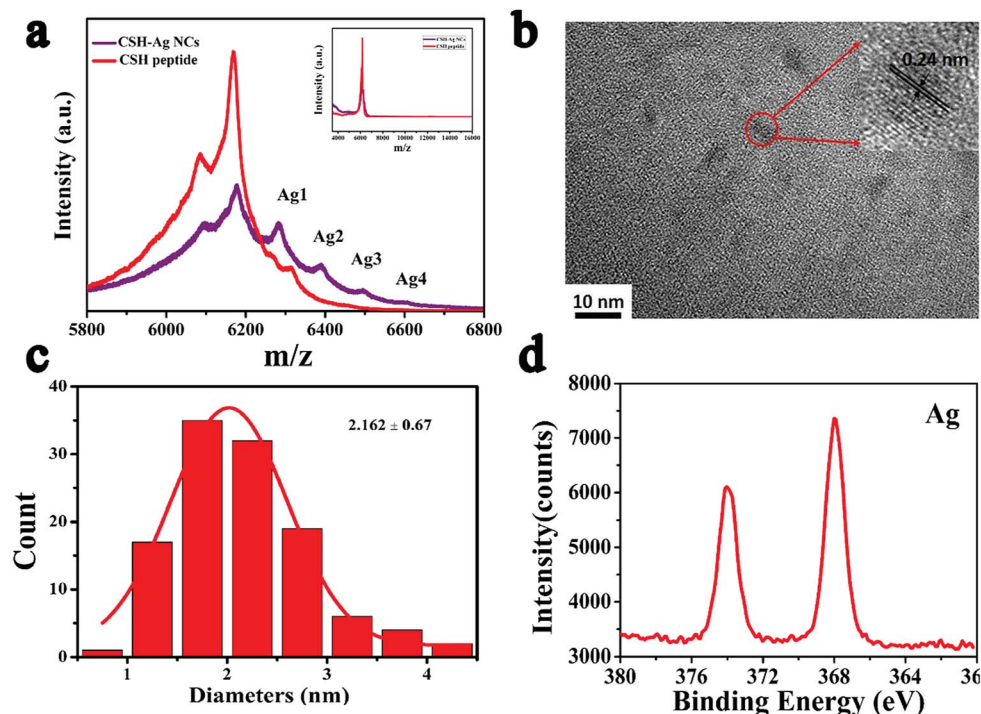
Fig. 2 The photographs of morphology and composition of CSH−Ag NCs. (a) Comparison of one CSH peptide (red) and peptide−Ag NCs (blue) by MALDI-TOF mass spectra, indicating the characteristic peaks are assigned to Ag1, Ag2, Ag3 and Ag4, respectively. The spacing gap between adjacent m/z peaks of CSH−Ag NCs (blue) is identified as ~108. (b) High resolution transmission electron microscopy (HRTEM) images showed the mean size of Ag NCs with 10 nm bar. The image of (inset) gives a lattice spacing of 0.24 nm corresponding to the (111) plane of Ag(0) (c) size distribution histogram of Ag NCs calculated from the TEM images by counting 116 number. (d) XPS spectrum confirms the CSH−Ag NCs with zero valence form in the Ag 3d region.

morphology can be explained by the interaction of electrically charged groups of the basic amino acid in the peptide, which prevents further aggregation of the Ag clusters.[30,31] Furthermore, the crystal form of the nanoparticles was examined, which indicated the existence of Ag (Fig. S3 in the ESI†). EDAX spectrum supported the presence of Ag and S of the CSH–Ag NCs in the sample along with the quantification data. The quantification data suggest that the Ag : S ratio is in good agreement with the theoretical value (Fig. S4 in the ESI†). To confirm the interaction between the peptide and Ag clusters, the composition and the chemical oxidation state of the Ag NCs were determined by X-ray photoelectron spectroscopy (XPS). As shown in Fig. 2d, the two intense peaks at ~368.12 eV and ~374.12 eV in the Ag 3d region of the XPS spectrum were assigned to the observed peaks of Ag 3d5/2 and Ag 3d3/2. This indicates the existence of Ag clusters with a zero valence form in the peptide–Ag cluster structure.

3.3.   Cellular imaging applications

To demonstrate the potential biomedical application of CSH–Ag NCs, the peptide–Ag NCs were used to verify their ability to stain cells. After incubating with murine preosteoblast MC3T3-E1 cells for 2 h, the Ag NCs observed by laser confocal fluorescence imaging show significant fluorescence emission in the live cells.[32,33] As shown in Fig. 3, the subcellular localization of the Ag clusters indicated that cell nuclei were primarily

occupied by Ag NCs because of their distinct color in the merged images. Notably, staining the organelles of cells is an important issue in clinical diagnosis and molecular studies, particularly for staining the nucleus in sub-cellular organelle imaging.[11,34] This result showed a novel approach for the easy fabrication and fluorescent staining of cell nuclei based on a silk fibroin derived peptide. Due the fact that the peptide–Ag NCs possess ultra-small size and a more positive charge, the reason for uptake and imaging of peptide–Ag NCs may be ascribed to transport through entry by endocytosis. Furthermore, we speculated that the peptide could act like a new class of cell penetrating peptides (CPPs) because of the abundant positive charges on the surface of the peptide.[34,35] The biological role of the peptide, however, should be investigated in future experiments.

3.4.   The test of cytotoxicity

To assess cellular toxicity of the CSH–Ag nanoclusters, their cellular cytotoxicity to the MC3T3-E1 cells was investigated using an MTT assay. As shown in Fig. S5 and S6,† five different concentrations of CSH–Ag NCs over five time intervals were tested and the apparent cytotoxicity was observed by determining the cell viability of the treated *versus* untreated cells. The results indicated that the CSH–Ag NCs caused a gradual decrease in cell viability in a time and dose dependent manner. Collectively, we speculate that Ag NCs functionalized by silk
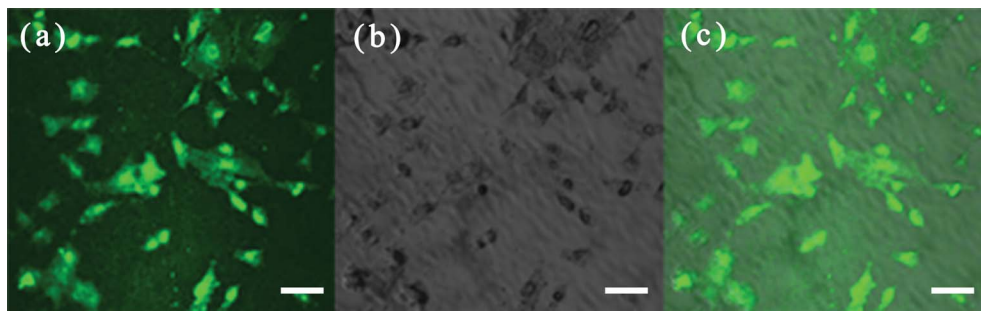
Fig. 3 The confocal microscope images of cellular staining of the CSH-Ag NCs in murine preosteoblast MC-3T3 cells with 405 nm excitation (a) fluorescent image of CSH-Ag NCs (b) bright field (c) merged image (scale bar: 50 μm).

fibroin derived peptide synergistically contribute to significant cytotoxicity effects in the MC3T3 cells.[34,36,37]

Conclusion

Herein, we report the first instance of the use of silk fibroin derived peptide from the *Bombyx mori* silkworm to synthesize Ag NCs *via* a one-pot green method. The as-synthesized Ag NCs with green emission showed a fluorescence peak at 550 nm in aqueous solution. The well-defined composition of peptide–Ag NCs was assigned as Ag1, Ag2, Ag3 and Ag4 using MALDI-TOF MS. The CSH–Ag NCs maintain stable and bright fluorescence in aqueous solution, which could be used for cellular imaging. Overall, this study verified the viability of amino acid sequence dependent peptides for the synthesis of Ag NCs and their synergistic functionality between the peptide/protein and Ag clusters in cell imaging. Because of the increasing interest of peptides in pharmaceutical research and development and the approximately 140 peptide therapeutics currently being evaluated in clinical trials,[38] future efforts could be devoted to explore to usage of functional peptides or proteins that originate from natural organisms. Moreover, it is desirable to understand the relationship of sequence specificity and growth mechanism of the metal cores. Inspired by this study, we believe that current research will intensively promote the rational exploration of silk fibroin resources and the fabrication of protein/peptide functionalized metal nanoclusters for biomedical applications guided by imaging.

Conflicts of interest

There is no competing conflict of interest to declare.

Acknowledgements

Notes and references

1 Y. Tao, M. Li, J. Ren and X. Qu, *Chem. Soc. Rev.*, 2015, **44**, 8636–8663.
2 M. Ammu and P. Thalappil, *Part. Part. Syst. Charact.*, 2014, **31**, 1017–1053.
3 S. Choi, R. M. Dickson and J. Yu, *Chem. Soc. Rev.*, 2012, **41**, 1867–1891.
4 Y. Lu and W. Chen, *Chem. Soc. Rev.*, 2012, **41**, 3594–3623.
5 Z. Luo, K. Zheng and J. Xie, *Chem. Commun.*, 2014, **50**, 5143–5155.
6 X. Hangxun and S. Kenneth Suslick, *Adv. Mater.*, 2010, **22**, 1078–1082.
7 I. Diez and R. H. A. Ras, *Nanoscale*, 2011, **3**, 1963–1970.
8 W. Wang, J. Li, J. Fan, W. Ning, B. Liu and C. Tong, *Sens. Actuators, B*, 2018, **267**, 174–180.
9 L. Shang and S. Dong, *Chem. Commun.*, 2008, 1088–1090, DOI: 10.1039/B717728C.
10 N. Makarava, A. Parfenov and I. V. Baskakov, *Biophys. J.*, 2005, **89**, 572–580.
11 Y. Junhua, S. A. Patel and R. M. Dickson, *Angew. Chem.*, 2007, **119**, 2074–2076.
12 A. Mathew, P. R. Sajanlal and T. Pradeep, *J. Mater. Chem.*, 2011, **21**, 11205–11212.
13 Y. Yu, Z. Luo, C. S. Teo, Y. N. Tan and J. Xie, *Chem. Commun.*, 2013, **49**, 9740–9742.
14 R. de la Rica and H. Matsui, *Chem. Soc. Rev.*, 2010, **39**, 3499–3509.
15 P. Radivojac, W. T. Clark, T. R. Oron, A. M. Schnoes, T. Wittkop, A. Sokolov, K. Graim, C. Funk, K. Verspoor, A. Ben-Hur, G. Pandey, J. M. Yunes, A. S. Talwalkar, S. Repo, M. L. Souza, D. Piovesan, R. Casadio, Z. Wang, J. Cheng, H. Fang, J. Gough, P. Koskinen, P. Törönen, J. Nokso-Koivisto, L. Holm, D. Cozzetto, D. W. A. Buchan, K. Bryson, D. T. Jones, B. Limaye, H. Inamdar, A. Datta,

S. K. Manjari, R. Joshi, M. Chitale, D. Kihara, A. M. Lisewski, S. Erdin, E. Venner, O. Lichtarge, R. Rentzsch, H. Yang, A. E. Romero, P. Bhat, A. Paccanaro, T. Hamp, R. Kaßner, S. Seemayer, E. Vicedo, C. Schaefer, D. Achten, F. Auer, A. Boehm, T. Braun, M. Hecht, M. Heron, P. Hönigschmid, T. A. Hopf, S. Kaufmann, M. Kiening, D. Krompass, C. Landerer, Y. Mahlich, M. Roos, J. Björne, T. Salakoski, A. Wong, H. Shatkay, F. Gatzmann, I. Sommer, M. N. Wass, M. J. E. Sternberg, N. Škunca, F. Supek, M. Bošnjak, P. Panov, S. Džeroski, T. Šmuc, Y. A. I. Kourmpetis, A. D. J. van Dijk, C. J. F. t. Braak, Y. Zhou, Q. Gong, X. Dong, W. Tian, M. Falda, P. Fontana, E. Lavezzo, B. Di Camillo, S. Toppo, L. Lan, N. Djuric, Y. Guo, S. Vucetic, A. Bairoch, M. Linial, P. C. Babbitt, S. E. Brenner, C. Orengo, B. Rost, S. D. Mooney and I. Friedberg, *Nat. Methods*, 2013, **10**, 221.

16 X. Yuan, Z. Luo, Q. Zhang, X. Zhang, Y. Zheng, J. Y. Lee and J. Xie, *ACS Nano*, 2011, **5**, 8800–8808.

17 K. Zheng, M. I. Setyawati, T.-P. Lim, D. T. Leong and J. Xie, *ACS Nano*, 2016, **10**, 7934–7942.

18 T. Zhou, Y. Huang, W. Li, Z. Cai, F. Luo, C. J. Yang and X. Chen, *Nanoscale*, 2012, **4**, 5312–5315.

19 S. S. Narayanan and S. K. Pal, *J. Phys. Chem. C*, 2008, **112**, 4874–4879.

20 C. Guo and J. Irudayaraj, *Anal. Chem.*, 2011, **83**, 2883–2889.

21 L. Shang, R. M. Dörlich, V. Trouillet, M. Bruns and G. Ulrich Nienhaus, *Nano Res.*, 2012, **5**, 531–542.

22 Y. Cui, Y. Wang, R. Liu, Z. Sun, Y. Wei, Y. Zhao and X. Gao, *ACS Nano*, 2011, **5**, 8684–8689.

23 V. A. Morozov and M. Y. Ogawa, *Inorg. Chem.*, 2013, **52**, 9166–9168.

24 N. Goswami, K. Zheng and J. Xie, *Nanoscale*, 2014, **6**, 13328–13347.

25 Y. Wang, Y. Cui, R. Liu, Y. Wei, X. Jiang, H. Zhu, L. Gao, Y. Zhao, Z. Chai and X. Gao, *Chem. Commun.*, 2013, **49**, 10724–10726.

26 Y. N. Tan, J. Y. Lee and D. I. C. Wang, *J. Am. Chem. Soc.*, 2010, **132**, 5677–5686.

27 J. Yu, S. A. Patel and R. M. Dickson, *Angew. Chem.*, 2007, **119**, 2074–2076.

28 Y. Teng, X. Yang, L. Han and E. Wang, *Chem.–Eur. J.*, 2014, **20**, 1111–1115.

29 X.-D. Zhang, J. Chen, Z. Luo, D. Wu, X. Shen, S.-S. Song, Y.-M. Sun, P.-X. Liu, J. Zhao, S. Huo, S. Fan, F. Fan, X.-J. Liang and J. Xie, *Adv. Healthcare Mater.*, 2014, **3**, 133–141.

30 Z. Li, H. Peng, J. Liu, Y. Tian, W. Yang, J. Yao, Z. Shao and X. Chen, *ACS Appl. Mater. Interfaces*, 2018, **10**, 83–90.

31 S. Ling, H. Liang, Z. Li, L. Ma, J. Yao, Z. Shao and X. Chen, *J. Mater. Chem. B*, 2016, **4**, 3643–3650.

32 S. Xu, H. Yang, K. Zhao, J. Li, L. Mei, Y. Xie and A. Deng, *RSC Adv.*, 2015, **5**, 11343–11348.

33 Z. Sun, Y. Wang, Y. Wei, R. Liu, H. Zhu, Y. Cui, Y. Zhao and X. Gao, *Chem. Commun.*, 2011, **47**, 11960–11962.

34 Y. Wang, Y. Cui, Y. Zhao, R. Liu, Z. Sun, W. Li and X. Gao, *Chem. Commun.*, 2012, **48**, 871–873.

35 D. M. Copolovici, K. Langel, E. Eriste and Ü. Langel, *ACS Nano*, 2014, **8**, 1972–1994.

36 C. Zhang, K. Wang, C. Li, Y. Liu, H. Fu, F. Pan and D. Cui, *J. Mater. Chem. B*, 2014, **2**, 6931–6938.

37 Y. Lu, Y. Chi, L. Feng, D. Yuhang, Z. Zhikun and Y. Dayong, *Small*, 2018, **14**, 1800185.

38 K. Fosgerau and T. Hoffmann, *Drug Discovery Today*, 2015, **20**, 122–128.